3 1176 00162 3421

NASA TM-81837

NASA Technical Memorandum 81837

NASA-TM-81837 19800020962

THE SPECTRAL OPACITY OF TRIATOMIC CARBON MEASURED IN A GRAPHITE TUBE FURNACE OVER THE 280 TO 600 NM WAVELENGTH RANGE

FOR REFERENCE

NOT TO BE TAKEN FROM THIS ROOM

WALTER L. SNOW AND WILLIAM L. WELLS

JULY 1980

LIBRARY COPY

NASA
National Aeronautics and Space Administration

Langley Research Center
Hampton, Virginia 23665

THE SPECTRAL OPACITY OF TRIATOMIC CARBON MEASURED IN A GRAPHITE TUBE FURNACE OVER THE 280 TO 600 nm WAVELENGTH RANGE

Walter L. Snow and William L. Wells
Langley Research Center

SUMMARY

The opacity of linear triatomic carbon (C_3) was measured in a graphite tube furnace from 280 to 600 nm to supplement the earlier measurements of Brewer and Engelke. The spectral cross section was estimated from the opacities using temperature profiles determined pyrometrically and a revised heat of formation (ΔH_0° = 198 kcal/mole). The cross section was found to be nonnegligible over the range 300-500 nm and the electronic oscillator strength based on the total cross section estimate was 0.02.

INTRODUCTION

The linear triatomic molecule C_3 has received a large amount of theoretical and experimental attention over the past several decades. The celebrated 4050 Å Swings bands were first observed in cometary spectra (refs. 1 and 2) and have subsequently been identified with the C_3 molecule by Clusius and Douglas (ref. 3) using laboratory methods. In graphite tube furnaces the bands are dwarfed by a strong underlying continuum which the work of Brewer and Engelke (ref. 4) associated with a blending of densely spaced rotational lines of triatomic carbon.

Thermodynamic interest hinges on the fact that linear chains of carbon atoms become increasingly important in treating high temperature equilibrium between graphite and its vapor. Thermodynamic potentials required to calculate equilibrium densities rely on the frequencies of vibrational modes. Such frequencies derived from both spectroscopic analysis and quantal calculations (refs. 5 and 6) differ greatly and enthalpies of formation reflect the variation. The state of affairs for C_3 has been summarized by Palmer (ref. 7) to 1967 and updated by Jones (ref. 8) recently.

The spectrum of C_3 has recently surfaced in a pure thermal engineering context in connection with designing crafts for outer planet missions (ref. 9). For the massive planets, radiative heating becomes comparable to and greater than the convective component. The phenolic carbon heat shields evolve large amounts of raw material which can form molecules capable of absorbing and thus filtering some of the troublesome energy directed toward the vehicle.

The purpose of this study was quite simply to extend the wavelength coverage of Brewer and Engelke from (370-490) to (290-600) nm. This was deemed

N80-29463#

especially desirable on the short wavelength side since the absorption is about 80 percent of maximum at 370 nm where the Brewer and Engelke data terminates. Our extended coverage also allows much easier accounting for particulate effects which were quite large in our case. The results presented here using equilibrium conditions pretty much support the conclusions of a recent more elaborate experimental study by Jones (ref. 8) using a shock tube.

EXPERIMENTAL[1]

Furnace

The main purpose of the study was to extend the relative spectrum of C_3 beyond the range covered by Brewer and Engelke under similar tube furnace conditions. The graphite tube furnace was a commercially available model used primarily for heat treatment and not intended for fundamental property measurements as are King furnaces. To construct and calibrate a research grade tube oven would have required an effort incommensurate with the stated purposes.

The graphite tube had a total length of 57.2 cm with a 5.1 cm internal diameter. The element was heated by the current flowing through it which was delivered through supporting graphite collars on either end. The entire metal drum which supported the configuration was packed with a graphite powder having the consistency of talcum to provide a relatively nonconducting thermal barrier.

The unit operated at atmospheric pressure with a low flow rate of argon to displace oxygen which would otherwise destroy the tube at the high temperatures required to generate substantial amounts of C_3. Although it is easy to accurately measure tube current and voltage, these variables do not in themselves establish the temperature distribution because the tube gets thinner and hence its resistance increases with usage time. This effect eventually leads to tube failure. Without tube shaping to compensate for thermal gradients which is done in more elaborate designs (ref. 10) the axial temperature distribution must be measured periodically in conjunction with spectral data acquisition. Operation to 3040° C precluded the use of thermocouples so an optical brightness pyrometer was used. To avoid having to view the furnace wall at grazing incidence, five graphite targets were placed at 5-cm intervals from the midpoint toward an end of the tube. The targets were small pedestals having 0.16-cm diameter rods supported in 0.95-cm diameter disks which served as their bases. The objects were expected to reach equilibrium with the cavity except close to the ends where severe gradients existed. Fortunately the hot inner zone was of primary interest. The disappearing filament pyrometer was very easy to sight and null out against these targets. When normalized to the midpoint temperature, t_c, the profile seemed to fall on a curve which was fitted by a quartic polynomial regression to

$$t/t_c = 0.99336 - 2.2211 \times 10^{-3}\, x^2 - 3.7868 \times 10^{-5}\, x^4 \qquad (1)$$

with x measured in inches from the midpoint and t in degrees C. Thereafter during the course of a run the midpoint value could be quickly determined by

[1]S. Franklin Edwards and William F. Stewart provided the furnace, laboratory space, and assistance in the pyrometry.

leaving the pyrometer focused on the center target and a reasonable estimate obtained for the complete axial profile with a single measurement.

Layout

This test involved determining the transmission of a hot gas filter so the setup was essentially that of a spectrophotometer. The boundary of the filter (furnace wall) was glowing hot and would swamp the effects due to the gas in the absence of lock-in discrimination. Figure 1 depicts the experimental arrangement. Light from a 100 W Hg short arc was collimated with a single quartz lens. A beam splitter directed part of the beam around the oven where it was labelled by a mechanical chopper before entering a spectrometer. The complementary beam was labelled by another mechanical chopper operating at a different frequency; passed through the oven and eventually was dispersed and subsequently detected with its associated lock-in amplifier. Outputs from the amplifiers could be directly fed to a ratiometer which in log mode delivered a signal directly proportional to the optical depth. Care was exercised to have each beam experience the same history so that spectral signatures of mirrors or splitters did not simulate gas transmission. A neutral screen was interposed from time to time in the course of a data sequence to ensure linearity of the system. The background lamp contained a significant amount of line structure and this made alinement of the furnace and reference beams very critical. This alinement was usually accomplished by removing the photomultiplier assembly and imaging the dispersed light onto a white card. The small pointlike images of the source in wavelengths corresponding to the Hg lines could then be superimposed by moving one of the steerable mirrors. This had to be done after initial furnace warmup because there was considerable refractive bending in the oven leg. Fortunately the bending did not change perceptibly once initial gradients were established. The system worked admirably once alined as can be seen in figure 2 where displayed is the radiometer signal along with the reference beam trace. The oven was relatively cool ($\leq 2200^{\circ}$ C) for this trace. Note the Na doublet in absorption indicating that the resolution was on the order of 5 angstroms (0.5 nm). The ratio remained essentially constant even when the background had pronounced spectral structure.

There were recurring problems with particulates (smoke) with this furnace. Some were traceable to asbestos gaskets which smoked when illuminated with the intense wall radiation. The same was true to a lesser extent with Teflon but the gasket problem was only resolved by use of soft copper. It was never possible to eliminate all the smoke when the oven was operated at the highest temperatures. The origins are presumed to be outgassing products from the graphite itself. Once cooled down the walls had whitish deposits having the appearance of leached salts. It was felt that the attenuation due to particulates could be reasonably accounted for as will be shown later. More troublesome was the possibility that the material would collect on windows during a scan since this would introduce a time-dependent cumulative bias. In most cases the windows remained clear through control of the gas flow which had entrance and exit ports in the window support flanges. When the windows were found to be clouded due to improper gas flow in the postrun transmission check, the data were not used.

The rolloff in sensitivity of the photomultiplier and the Hg light source combined to limit the longer wavelength measurements to 600 nm. Fused silica optics (including beam splitters) enabled UV extension to 200 nm but source intensity limited practical measurements to 280 nm.

DATA INTERPRETATION

Figure 3 is a retracing of raw data obtained when the furnace was operated at a midpoint temperature of 2910^{o} C. The readings were taken on a dual pen recorder. One channel monitored the background with deflection from bottom to top. The gain was increased by a factor of 10 for the 440-600 nm range where the signals were weaker. The second channel monitored the ratiometer output, i.e., $\log_{10}(I/I_o)$ where I_o is the beam intensity through the by-pass leg and I is the intensity through the furnace leg. The relatively rapid spectral variation of atomic (e.g., Na) and diatomic (C_2, CN) species allowed their easy identification and "removal" from the records. For the pathlengths considered, the relatively broad C_3 continuum centered around 400 nm is evident even at this low temperature.

The interpretation of results involved two distinct steps. First, it was necessary to unravel the absorption contribution of C_3 by exploiting specie wavelength-signatures. This was easy for sharp features such as atomic and diatomic constituents, and the prior work of Brewer and Engelke greatly facilitated the identification of C_3. Particulate contributions were only slightly more complicated as will be discussed shortly. The second stage of interpretation involved estimating the strength of the triatomic system and this entailed an estimate of the total number of C_3 molecules contributing to the observation. This was done using the measured temperature distribution of the furnace in conjunction with chosen thermodynamic potentials.

Each component in the oven acted independently to attenuate the lamp radiation. If T represents transmission then at any wavelength

$$T^{tot.} = T^{C3} \cdot T^{part.} \cdot T^{C2} \cdot T^{Na} \cdot \ldots \qquad (2)$$

The regions perturbed by atomic and diatomic components could be easily removed by extrapolating the adjacent background as shown with the dashed lines in figure 3. What remained was a relatively "slow" dependence fairly well characterized by plotting points every 100 angstroms (10 nm). This was done in figure 4(a) along with the measured system response. It seemed reasonable to extrapolate the background between 300 and, say, 520 nm to identify the C_3 contribution. The remaining attenuation increasing strongly to the violet is suggestive of particulate (Mie) scattering by small particles. In the gas heavily laden with C atoms it is not unreasonable to expect particulate carbon to form and "smoke" could be observed during some of the runs. It was not known whether any or all of this was carbon.

In general the transmission due to species i is written as

$$T_\lambda^{\,i} = \exp\left(- \int_o^L n^i(x)\, \sigma_\lambda^{\,i}\, dx \right) = \exp\left(-N^i\, \sigma_\lambda^{\,i}\right) \qquad (3)$$

where $n^i(x)$ is the local number density of absorbers in cm^{-3} and $\sigma_\lambda{}^i$ is the spectral extinction cross section in cm^2. $N^i \equiv \int_o^L n^i(x)\,dx$ represents the total particle load along the pathlength L. The calculation of extinction cross section for spherical particles of radius a and refractive index $m = n_1 - \underline{i}n_2$ is well known. The formulae are series combinations of spherical Bessel functions and their spatial derivatives. The formulae of Wickramasinghe (ref. 11) were programed in BASIC for a calculator for this work. The natural dimensionless variable for such calculations is $x = 2\pi a/\lambda$, the so-called size parameter. Precise modeling requires an accurate knowledge of the size distribution of the particulates. This was not known, so an estimate was made based on McDonald's (ref. 12) observation that in an oxygen-starved environment of C_2 or C_3 spontaneous nucleation results in 2 nm diameter particles which aggregate into "popcorn balls" 10-50 nm in diameter. Here, 20 nm was chosen as a representative diameter consistent with this range and the choices of other workers calculating carbon opacity (see refs. 13, 14).

For the 20 nm particles the small-x expansions of the Mie cross sections are sufficient to help to display the dominant wavelength dependence. In particular

$$\sigma^{abs}(\lambda;a) = \pi a^2 (-4x)\ \mathrm{Im}\left(\frac{m^2 - 1}{m^2 + 2}\right) + \ldots \tag{4a}$$

and

$$\sigma^{sca}(\lambda;a) = \pi a^2 \frac{8}{3} x^4 \left|\frac{m^2 - 1}{m^2 + 2}\right|^2 + \ldots \tag{4b}$$

These expressions can be explicitly written in terms of particle radius and wavelength as follows:

$$\sigma^{abs}(\lambda;a) = \pi a^2\, 4\pi a \frac{n_1 n_2}{\left[n_2{}^4 + \left(2n_1{}^2 - 4\right)n_2{}^2 + n_1{}^4 + 4n_1{}^2 + 4\right]\lambda} \equiv \frac{p(\lambda;a)}{\lambda} \tag{5a}$$

and

$$\sigma^{sca}(\lambda;a) = \pi a^2 \frac{128\pi^4 a^4}{3} \frac{n_2{}^4 + \left(2n_1{}^2 + 2\right)n_2{}^2 + n_1{}^4 - 2n_1{}^2 + 1}{\left[n_2{}^4 + \left(2n_1{}^2 - 4\right)n_2{}^2 + n_1{}^4 + 4n_1{}^2 + 4\right]\lambda^4} \equiv \frac{q(\lambda;a)}{\lambda} \tag{5b}$$

For nonabsorbing particles $n_2 = 0$ and only the Rayleigh scattering remains. For carbon the index does have an appreciable imaginary component. The index varies from $1.552-0.726\,\underline{i}$ at 300 nm to $1.807-0.803\,\underline{i}$ at 580 nm according to the formulae of Stull and Plass (ref. 13).

The removal of the particulate contribution could then be effected as follows. After accounting for the system response the transmission at 580 nm was totally attributed to particulate carbon. The equation (3) could be used to calculate $N^{part.\ C}$. This particle load in conjunction with the scattering cross section could be used to compute the transmission at 300 nm. In general the method overpredicted the extinction, so it was decided that subject to the approximations particulate carbon was not the sole contributor to the smoke. The dominant wavelength dependence was $1/\lambda^4$, suggesting a scatterer with only a real index. (See equation (5b) with $n_2 = 0$.) An unknown component X having a real index 1.5 with particle diameter of 20 nm was assumed.

The observation at the two wavelengths, 300 nm and 580 nm, were used to solve the following simultaneous equations for $N^{part.\ C}$ and $N^{part.\ X}$.

$$\begin{aligned} \ell n\ T_{300} &= -N^{part.\ C}\ \sigma_{300}^{C} - N^{part.\ X}\ \sigma_{300}^{X} \\ \ell n\ T_{580} &= -N^{part.\ C}\ \sigma_{580}^{C} - N^{part.\ X}\ \sigma_{580}^{X} \end{aligned} \tag{6}$$

Typically $N^{part.\ X}$ was on the order of 10^{12}-10^{13} while $N^{part.\ C}$ was at least two orders of magnitude lower and often was not detectable at all. Having determined the particulate load it was then possible to compute the particulate extinction even in the regions where C_3 was dominant. An example is shown in figure 4(b). It should be emphasized that this methodology was simply used to provide a reasonable interpolating function for the background to evaluate the true C_3 contribution. An experiment to actually classify or quantitatively identify the particulate composition would be much more difficult although it would incorporate similar Mie calculations.

The C_3 opacity is plotted in figure 5 for several sets of data. Opacity is $-\ell n\ T$ and the figure shows how the system evolves with increasing optical depth. The individual curves are marked with the measured integrated absorption of the $C_2(\Delta v = 0)$ Swan system and the midpoint temperature t_c consistent with this value. The second phase of the problem, to translate measured opacities into estimates of the absorption cross section, will now be addressed.

Since an isothermal slab of C_3 was not available to work with, the interpretation of results in terms of absolute cross sections was indirect and certainly of less significance than the raw opacities. Some means of estimating the line integral of the pertinent particle density over the length of the furnace was needed. This required both temperature distribution and thermodynamic potentials, which allow calculation of equilibrium densities as a function of temperature. The midpoint temperature was determined before and after each trace using an optical pyrometer. The measured temperatures sometimes differed by 20 degrees or so and it was desirable to have a kind of internal standard with which to order the data. The $\Delta v = 0$ Swan system

of C_2 in the vicinity of 510 nm was quite suitable because it appeared whenever C_3 was measurable. This system is labelled on figure 3. The integrated absorption of a single vibrational band is given by

$$S_{[\bar{\nu}]}(e'v',e''v'') = \frac{8\pi^3}{3hc} N(e''v'') \langle\bar{\nu}\rangle \overline{R_e^2} \mathcal{S}(e'v',e''v'') \tag{7}$$

with

$$N(e''v'') = \frac{N(e'')}{Q_{vib}} e^{-hcG(v'')/kT}$$

$$Q_{vib} = \sum_{v''} e^{-hcG(v'')/kT}$$

and

$$\mathcal{S}(e'v',e''v'') = |\langle\psi_{v'}|\psi_{v''}\rangle|^2 = q_{v'v''}.$$

Double primes refer to the lower states, $q_{v'v''}$ is the Franck-Condon factor, $\overline{R_e^2}$ the mean square electronic transition moment, and N the pertinent number density. The vibrational term values are given by

$$G(v) = \omega_e(v+\tfrac{1}{2}) - \omega_e x_e(v+\tfrac{1}{2})^2 + \omega_e y_e(v+\tfrac{1}{2})^3 + \omega_e z_e(v+\tfrac{1}{2})^4. \tag{8}$$

The integrated absorption for an entire $v' - v''$ system is found by summing equation (7) over v', v''. For the $\Delta v = 0$ sequence

$$\sum_{v'v''} S_{[\bar{\nu}]}(e'v', e''v'')\delta_{v'v''} = \frac{8\pi^3}{3hc} \langle\bar{\nu}\rangle \overline{R_e^2} \sum_{v''=0}^{10} N(e''v'')q_{v''v''} \tag{9}$$

$$= \frac{8\pi^3}{3hc} \langle\bar{\nu}\rangle \overline{R_e^2} \frac{N_{e''}(T(x))}{Q_{vib}(T(x))} \sum_{v''=0}^{10} e^{\frac{-hcG''(v'')}{kT(x)}} q_{v''v''}$$

The explicit temperature dependence has been displayed. To compare with observation it is necessary to integrate over the pathlength through the oven

using equation (1) for the temperature distribution. The summation is truncated at level 10 due to unavailability of measurable Franck-Condon factors beyond v = 0. The pertinent constants for the Swan system are recorded in table 1 and taken from McCallum et al. (ref. 15). The transition moment values are scattered and recently reviewed by Nicholls and Cooper (ref. 16). The cited values (with their error estimates) are bounded by 0.02 and 4.56. The majority of shock tube and furnace determinations now favor a value in the range 3.0-4.0.[1] This variation in transition moment of course scales the integrated absorption as indicated in figure 6. The abscissa is the midpoint temperature, which with the normalized distribution specifies the entire temperature profile of the oven. The horizontal bars represent the difference in temperatures as measured immediately before and after the spectral scan. Based on these measurements $\overline{R_e^2} = 0.4$ has been chosen to represent the data reported here. This choice is shown dashed on figure 6. This value falls below other currently accepted furnace and shock tube determinations by nearly an order of magnitude. To shift the C_2 measurements into agreement with the current modal value would require a temperature bias error on the order of 150°C. The pyrometer calibration correction (∿10°C), brightness to true conversion assuming graphite target emissivity of 0.8 (∿100°C), and residual [measured minus calculated temperature using equation (1)] (∿ ± 25°C with one deviation as high as 80°C) coupled with run to run variations are expected to account for scatter but should not consistently bias the interpretation in one direction.

The simple expression used to characterize the temperature profile is certainly not expected to hold rigidly. The actual profile might "flatten out" for example as the furnace approaches failure. This could account for the roll-off at high temperatures. If the C_2 data are made to conform with shock tube data then the molecular concentrations were overestimated by a factor of 10. This would raise the derived C_3 cross sections by the same factor barring compensation from the uncertainty in formation enthalpy for C_3. Considerably less significance is attached to the data when rendered absolute because of the nature of this experiment. This applies of course to the C_3 data as well. Having adopted a one-to-one correspondence between the measured integrated absorption and temperature, the method was used to determine the temperature t_c characterizing the data block.

Equilibrium densities for this work were calculated using a computer code called ACE (ref. 17) with JANAF (ref. 18) values for thermodynamic properties of C_2. To calculate the C_3 molecular concentration also required an equilibrium calculation based on a rather broad range of available heats of formation for this molecule. The equilibrium densities of C_3 vs. temperature for a range of formation enthalpies are shown in figure 7. As pointed out in the introduction, Brewer and Engelke used $\Delta H_0°$= 188 kcal/mole and the recent review of Jones favors 198.0 kcal/mole. The latter value, shown dashed in the figure, was also adopted for this work along with auxiliary potentials from Lee and Sanborn (ref. 19) to compute the total molecular concentration for the data reduction.

[1] Hagen's 1963 King furnace result is incorrectly listed and should be 3.67 as it now appears in High Temperature Science 11, 223-264 (1979).

It might be appropriate to briefly summarize the steps used to interpret the data. Pyrometric determinations of the temperature profile in the oven and measurements of integrated absorption of the $\Delta v = 0$ sequence of the C_2 Swan system provided correlation of a measured temperature distribution with a macroscopic spectral measurement similar to the one to be determined. This temperature was used to calculate the total C_3 concentration which corresponded to measured opacities. These opacities were determined in turn by removing the system response and particulate effects.

The results of 11 independent data sets taken over the period of a month are listed in table 2 and plotted in figure 8. The "error bars" represent ± one unbiased standard deviation and thus reflect measurement error rather than accuracy, which would require quantitative judgements on thermochemical and spectroscopic constants.

The opacities observed by Brewer and Engelke are plotted in figure 5. Since the measurements reported here and those of Jones indicate very low values at 500 nm the Brewer results were also plotted assuming that their value at 500 nm was entirely due to particulate extinction with 20 nm radius particles and index 1.50. These "corrected" values seem to be consistent with the data reported here. Brewer and Engelke argue against particulates and the authors do not presume to reinterpret their results, but it is felt that the extension to the near UV as in this work made it easier to identify the presence of a solid constituent. The particulate density required to "correct" their values was 5×10^{11} cm^{-3}, which is orders of magnitude below the C_3 densities. The particulates are simply much more efficient.

For engineering purposes it is sometimes helpful to crudely characterize the influence of one spectral feature relative to another at the expense of compromising a definition. The oscillator strength or transition probability is indeed a fundamental constant relating to transitions between states. Experimenters rarely have access to such detail and must contend with complicated averages over a multitude of transitions. Tatum states (ref. 20) succinctly

> "However, the rigorous calculation of the effective transition probability and frequency of a band system is so fraught with difficulties that it is doubtful whether it has ever been done. Indeed, when the Boltzmann factors are introduced into the equations, we find that the transition probability is temperature-dependent(!) and further that the "effective frequency" is different in absorption and in emission. The same sort of remarks apply to attempts to define a single value for the oscillator strength of a band system. We conclude that such statements as 'the f-value of the system is 0.3' have rather little meaning, and we propose that such expressions as 'oscillator strength of the system,' 'electronic oscillator strength,' and 'f_{el}' be dropped from the terminology of molecular spectroscopy."

Having paid homage to reason and with blatant disregard for logical argument the authors relate the integral of the absorption cross section to the oscillator strength by (ref. 21)

$$f_e = 1.13 \times 10^{12} \int_0^\infty \sigma_{\bar{\nu}}\, d\bar{\nu} \qquad (10)$$

This corresponds to a radiative lifetime of

$$\tau_{(1/e)} = 1.5/\bar{\nu}^2 f$$

with $\bar{\nu}$ in wavenumbers and taken as 24514 cm^{-1} for the C_3 system. The data plotted in figure 8 correspond to $f = 0.020$ and $\tau_{(1/e)} = 1.3 \times 10^{-7}$ s. These values are compared with other estimates in table 3 and are seen to be consistent with other work.

CONCLUDING REMARKS

A graphite wall furnace experiment was conducted to measure the spectral opacity of the C_3 molecule over the 280 to 600 nm range.

Because of furnace wall brightness and refractive bending of the light source beam within the furnace the optical system alinement was difficult, but by judicious use of electronic equipment and realinement after furnace operation, conditions were achieved for which the transmission of the furnace gases could be measured. Although particulate matter (smoke) of unknown origin sometimes interferred with the measurements, it was possible to account for the effect and remove it from the data.

The spectral opacity of the C_3 system increased with temperature over the measured range from 2993-3333 K (2720-3060 C) and the maximum opacity occurred near 400 nm wavelength. The results of this work agree qualitatively with that of Brewer and Engelke and showed appreciable C_3 absorption for a wider spectral range than their experiment covered. This study indicated that the C_3 opacity is significant in the spectral range from about 300 to 470 nm.

Using the $\Delta v = 0$ Swan system of C_2 in the vicinity of 510 nm as an internal standard for determination of integrated particle density, the C_3 absorption cross section was found to be significant and the electronic oscillator strength based on the estimated cross section was calculated to be 0.02.

REFERENCES

1. Huggins, W.: Proc. Roy. Soc. (London), vol. 33, 1882, p. 1.

2. Swings, R.: Rev. Mod. Phys., vol. 14, 1942, p. 190.

3. Clusuis, K. and Douglas, A. E.: J. Chem. Phys., vol. 32, 1954, p. 319.

4. Brewer, L. and Engelke, J. L.: J. Chem. Phys., vol. 36, 1962, p. 992.

5. Pitzer, K. S. and Clementi, E.: Large Molecules in Carbon Vapor. J. American Chem. Soc., vol. 81, no. 17, 1959, pp. 4477-4485.

6. Peric-Radic, J.; Romelt, J.; and Peyerimhoff, S. D.: Configuration Interaction Calculation of the Potential Curves for the C_3 Molecule in Its Ground and Lowest-Lying π_u States. Chem. Phys. Let., vol. 50, no. 2, 1977, pp. 344-350.

7. Palmer, Howard B. and Shelef, Mordecai: Vaporization of Carbon. Chem. and Phys. of Carbon, vol. 4, Phillip L. Walker, Jr., ed., Marcal Dekker, Inc., 1968, pp. 85-135.

8a. Jones, Jim J.: The Optical Absorption of Triatomic Carbon C_3 for the Wavelength Range 260 to 560 nm. NASA TP 1141, 1978.

8b. Cooper, D. M. and Jones, J. J.: An Experimental Determination of the Cross Section of the Swings Band System of C_3. J. Quant. Spectros. Radiat. Transfer, vol. 22, 1979, pp. 201-208.

9. Moss, James N.; Anderson, E. Clay; and Bolz, Charles W., Jr.: Viscous-Shock-Layer Solution With Radiation and Ablation Injection for Jovian Entry. AIAA Paper 75-671, May 1975.

10. Brewer, L.; Gilles, P. W.; and Jenkins, F. A.: The Vapor Pressure and Heat of Sublimation of Graphite. J. Chem. Phys., vol. 16, no. 8, 1948, pp. 797-807.

11. Wickramasinghe, N. C.: Light Scattering Functions for Small Particles With Applications in Astronomy. John Wiley and Sons, New York, 1973.

12. McDonald, J. E.: Visibility Reduction Due to Jet Exhaust Carbon Particles. J. Appl. Meteorology, vol. 1, 1962, pp. 391-398.

13. Stull, V. and Plass, G. N.: Emissivity of Dispersed Carbon Particles. J. Opt. Soc. America, vol. 50, no. 2, February 1960, pp. 121-129.

14. Main, Roger P. and Bauer, Ernest: Opacities of Carbon-Air Mixtures at Temperatures From 3000-10,000° K. J. Quant. Spectros. and Radiat. Transfer, vol. 6, no. 1, January/February 1966, pp. 1-30.

15. McCallum, J. C.; Jarmain, W. R.; and Nicholls, R. W.: Spectroscopic Report No. 1. Centre for Research in Experimental Space Science, New York University, Toronto, 1970.

16. Cooper, D. M. and Nicholls, W. R.: Measurements of the Electronic Transition Moments in C_2-Band Systems. J. Quant. Spectros. Radiat. Transfer, vol. 15, 1975, pp. 139-150.

17. Powars, Charles A. and Kendall, Robert M.: User's Manual--Aerotherm Chemical Equilibrium (ACE) Computer Program. Aerotherm Corp., May 1969.

18. JANAF Thermochemical Tables. NSRDS-NBS 37, U.S. Dept. of Commerce, June 1971.

19. Lee, E. L. and Sanborn, R. H.: Extended and Improved Thermal Functions for the Gaseous Carbon Species C_1-C_7 From 298 to 10,000° K. High Temp. Sci., vol. 5, no. 6, December 1973, pp. 438-453.

20. Tatum, J. B.: The Interpretation of Intensities in Diatomic Molecular Spectra. The Astrophysical Journal Supplement Series, Supplement 124, Vol. XIV, March 1967, pp. 21-56.

21. Griem, H. R.: Plasma Spectroscopy. Chapter 2, McGraw-Hill Book Co., 1964.

22. Barger, R. L. and Broida, H. P.: J. Chem. Phys, vol. 37, p. 1152 and vol. 43, 1965, p. 2364.

TABLE 1.- CONSTANTS (ref. 15) FOR C_2 SWAN $\Delta v = 0$ SEQUENCE

(Designation: $(A^3\pi_g - X^3\pi_u)$ (see ref. 15) or $(d^3\pi_g - a^3\pi_u)$ (see ref. 16)

Reduced mass: 6.00194 amu

$\omega_e'' = 1641.35\ cm^{-1}$, $\omega_e' = 1788.22\ cm^{-1}$

$\omega_e x_e'' = 11.67\ cm^{-1}$, $\omega_e x_e' = 16.44\ cm^{-1}$

$\omega_e y_e'' = 0.0$, $\omega_e y_e' = -0.5067\ cm^{-1}$

$D_e'' = 45000.0\ cm^{-1}$, $D_e' = 36000.0\ cm^{-1}$

$q_{v'v''}$ weighted wavelength = 511.6 nm

$\overline{R_e^2} = 0.4$ a.u. (see fig. 8)

v' - v''	λ; nm	$q_{v'v''}$
0-0	516.0	0.724E0
1-1	512.4	0.330E0
2-2	509.3	0.117E0
3-3	506.6	0.223E-1
4-4	504.4	0.175E-4
5-5	502.9	0.148E-1
6-6	502.0	0.425E-1
7-7	501.9	0.680E-1
8-8	502.5	0.834E-1
9-9	504.1	0.861E-1
10-10	506.7	0.776E-1

TABLE 2.- MEAN AND UNBIASED STANDARD DEVIATIONS FOR C_3 CROSS SECTION BASED ON ELEVEN INDEPENDENT DATA SETS

	σ, cm^2				
λ, nm	$<\sigma>$	<s.d.>	λ,nm	$<\sigma>$	<s.d.>
310	5.17E-19	1.66E-19	410	2.22E-18	5.59E-19
320	8.60E-19	3.24E-19	420	1.42E-18	4.71E-19
330	1.23E-18	4.15E-19	430	8.22E-19	1.88E-19
340	1.53E-18	3.13E-19	440	3.92E-19	2.49E-19
350	1.86E-18	2.86E-19	450	2.40E-19	1.01E-19
360	2.12E-18	3.16E-19	460	1.61E-19	5.39E-20
370	2.43E-18	4.25E-19	470	8.58E-20	3.99E-20
380	2.92E-18	4.28E-19	480	5.84E-20	5.00E-20
390	3.25E-18	7.21E-19	490	3.49E-20	8.86E-21
400	3.20E-18	9.56E-19	500	2.73E-20	1.73E-20

TABLE 3.- COMPARISON OF ELECTRONIC OSCILLATOR STRENGTHS FOR C_3

	f_e	τ(1/e)
This expt.	0.020	1.3E-7 s.
Jones (ref. 8a) (expt.)	.062-.036	
Cooper (ref. 8b) (expt.)	0.033	
Brewer (ref. 4) (expt.)	0.13	
Perić-Radić (ref. 6) (calc.)	0.061	4.18E-8 s.
Barger (ref. 22) (expt.)	0.06	

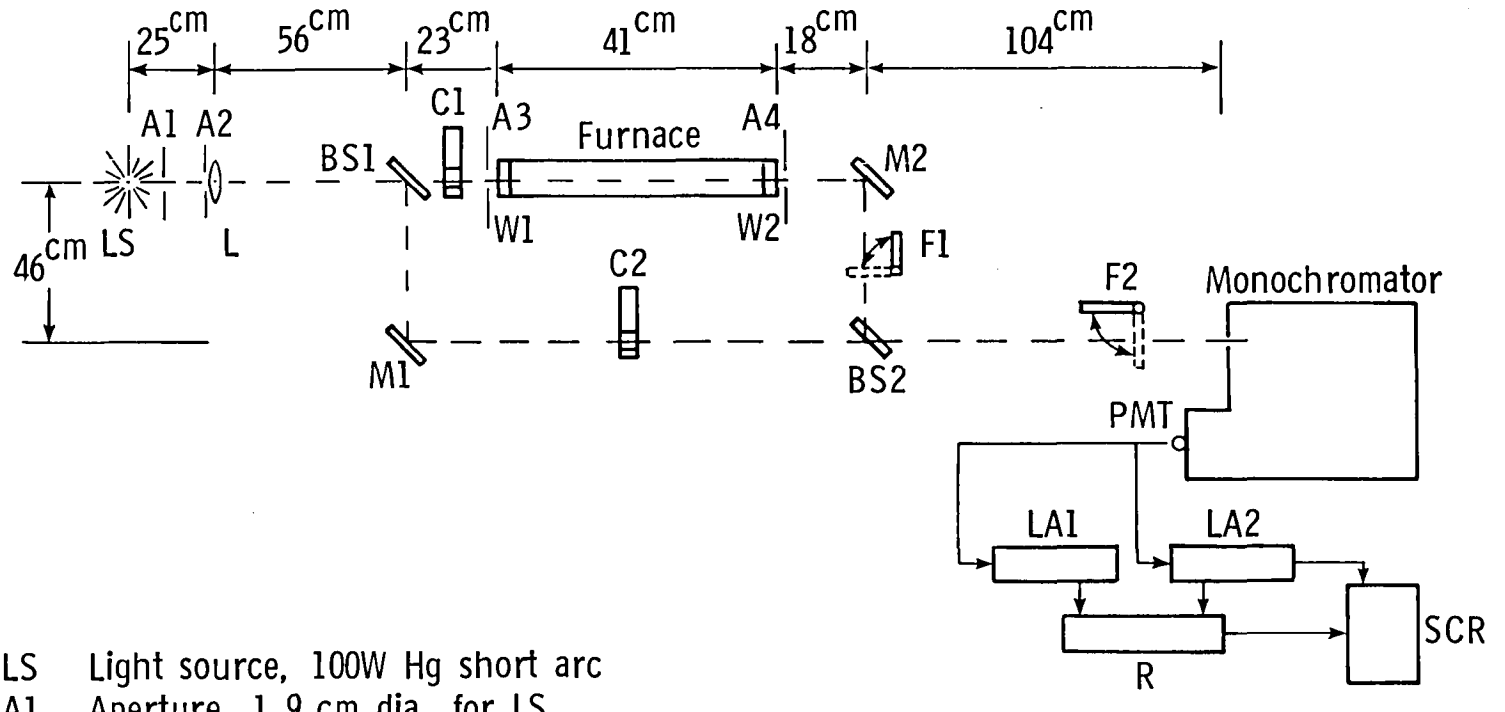

LS	Light source, 100W Hg short arc
A1	Aperture, 1.9 cm dia. for LS
A2	Aperture, 0.32 × 1.27 cm for L
L	Lens, collimator, quartz 2.54 cm dia., f = 25 cm (ORIEL A-11-641-40)
BS1, BS2	Beam splitter (ORIEL A-43-564-60-3)
M1, M2	Mirror, front surface
C1	Light chopper (PAR model 125)
C2	Light chopper (Brower model 322)
A3, A4	Aperture, 1.9 cm dia. for furnace wall mask

W1, W2	Window, quartz
F1	Filter, screen 33 percent trans.
F2	Filter, order sorter, 2 mm thick (Schott WG345)
SCR	2-pen chart recorder (HP 7132 A)
LA1, LA2	Lock-in amplifier (PAR model 128A)
R	Ratiometer (PAR model 188)
Furnace	Graphite tube, 5.08 cm I.D. (Pereco model CT-215 118)
Monochromator	Scanning 0.5-m Czerny-Turner (McPherson model 216.5)
PMT	Photomultiplier tube, 1P28

Figure 1.- Electro-optical arrangement for determining C_3 absorption in a graphite furnace.

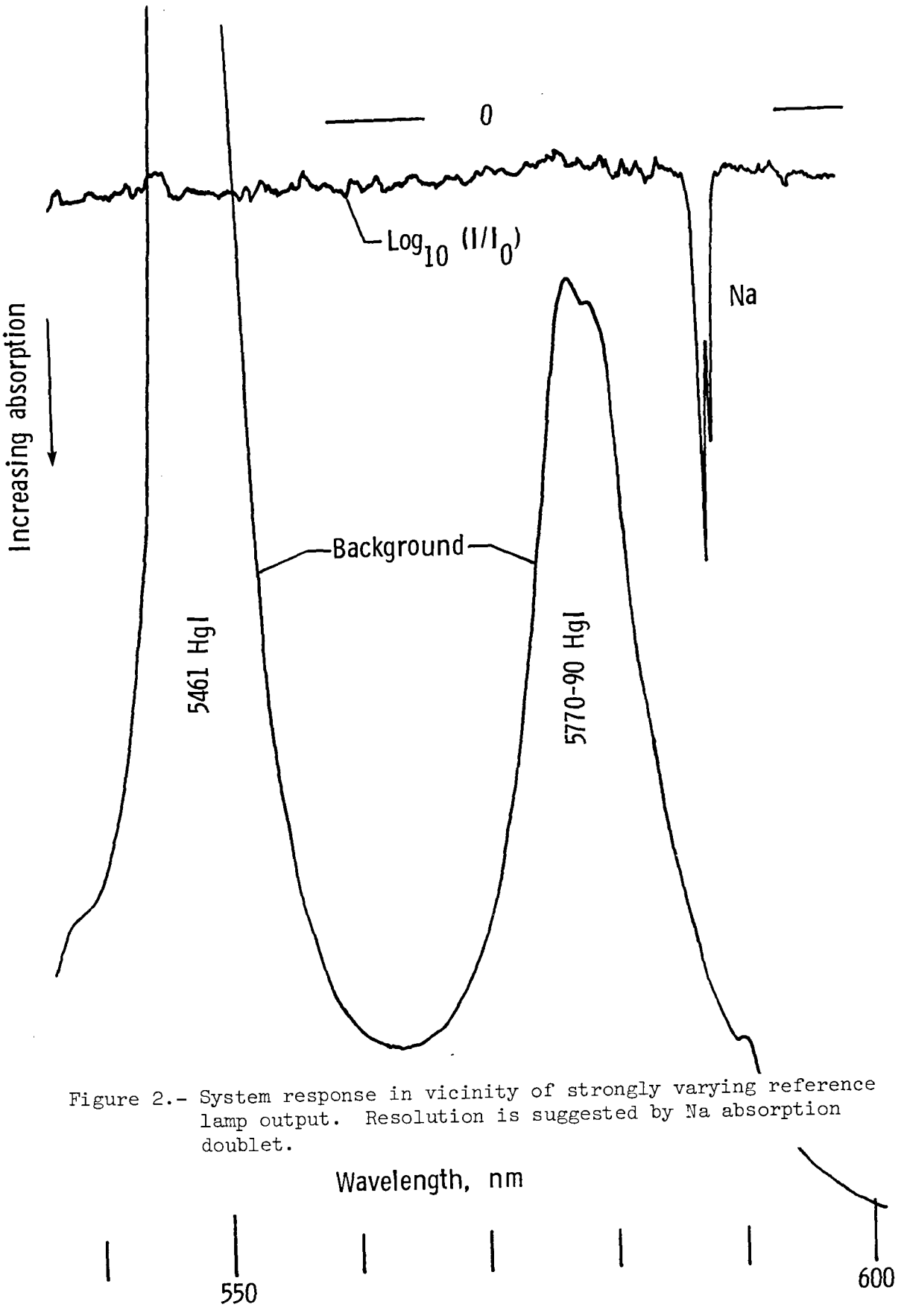

Figure 2.- System response in vicinity of strongly varying reference lamp output. Resolution is suggested by Na absorption doublet.

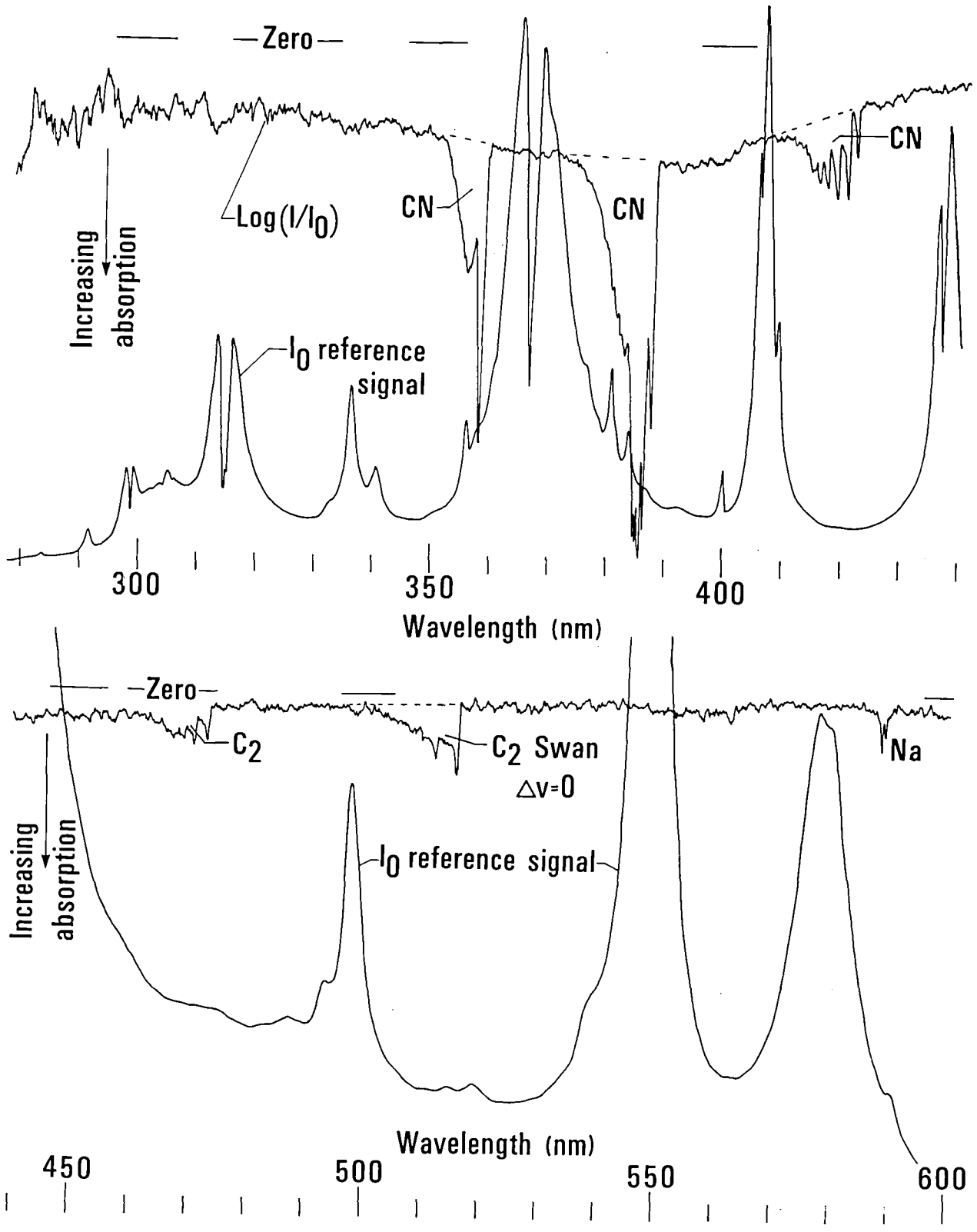

Figure 3.- Representative data trace showing the onset of C_3 absorption t_c = 2910°C.

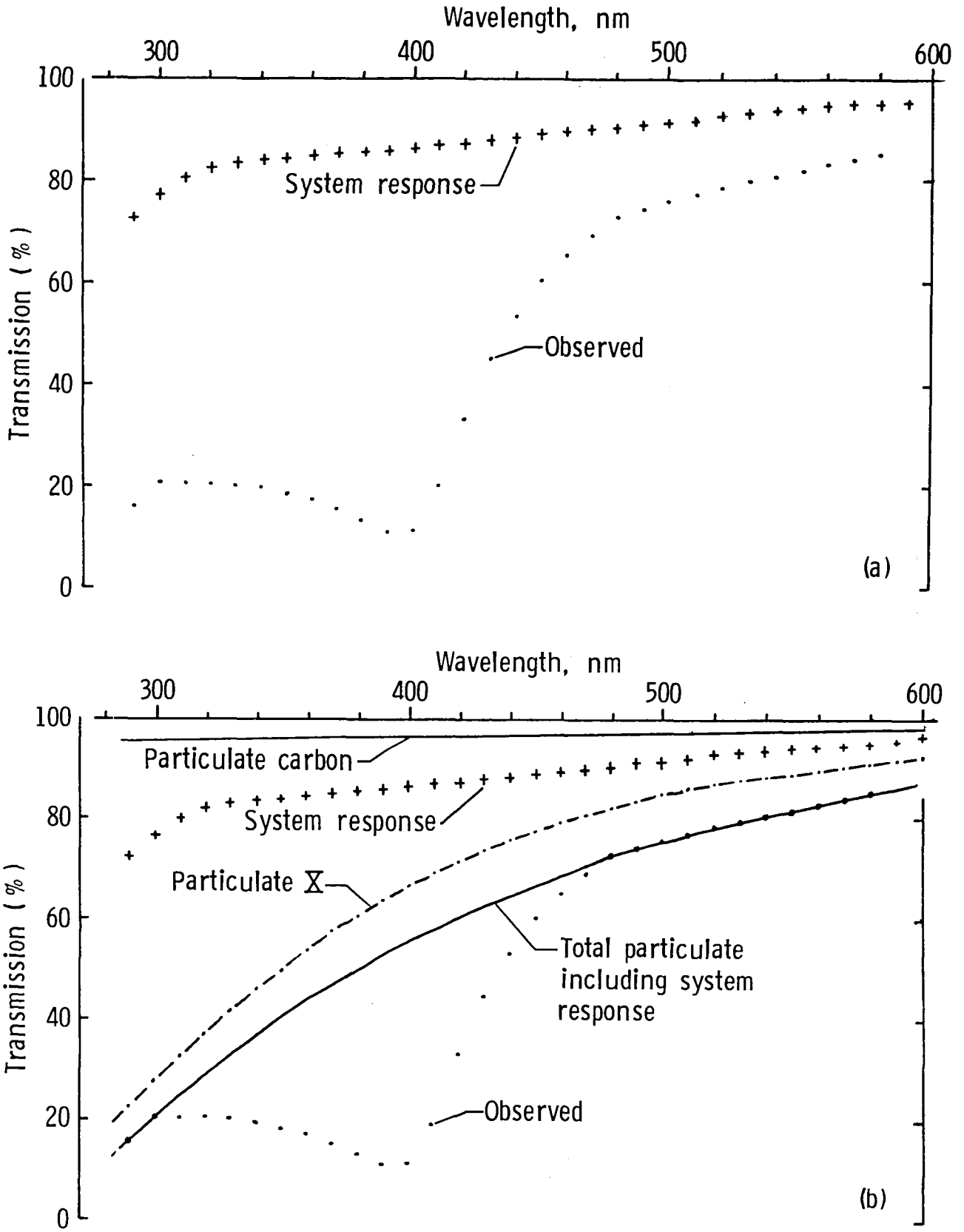

Figure 4.- Furnace transmission at t_c = 3060°C. (a) Observation after deleting known atomic and diatomic contributions. (b) Explicit dependence of particulate contributions to the observed transmission.

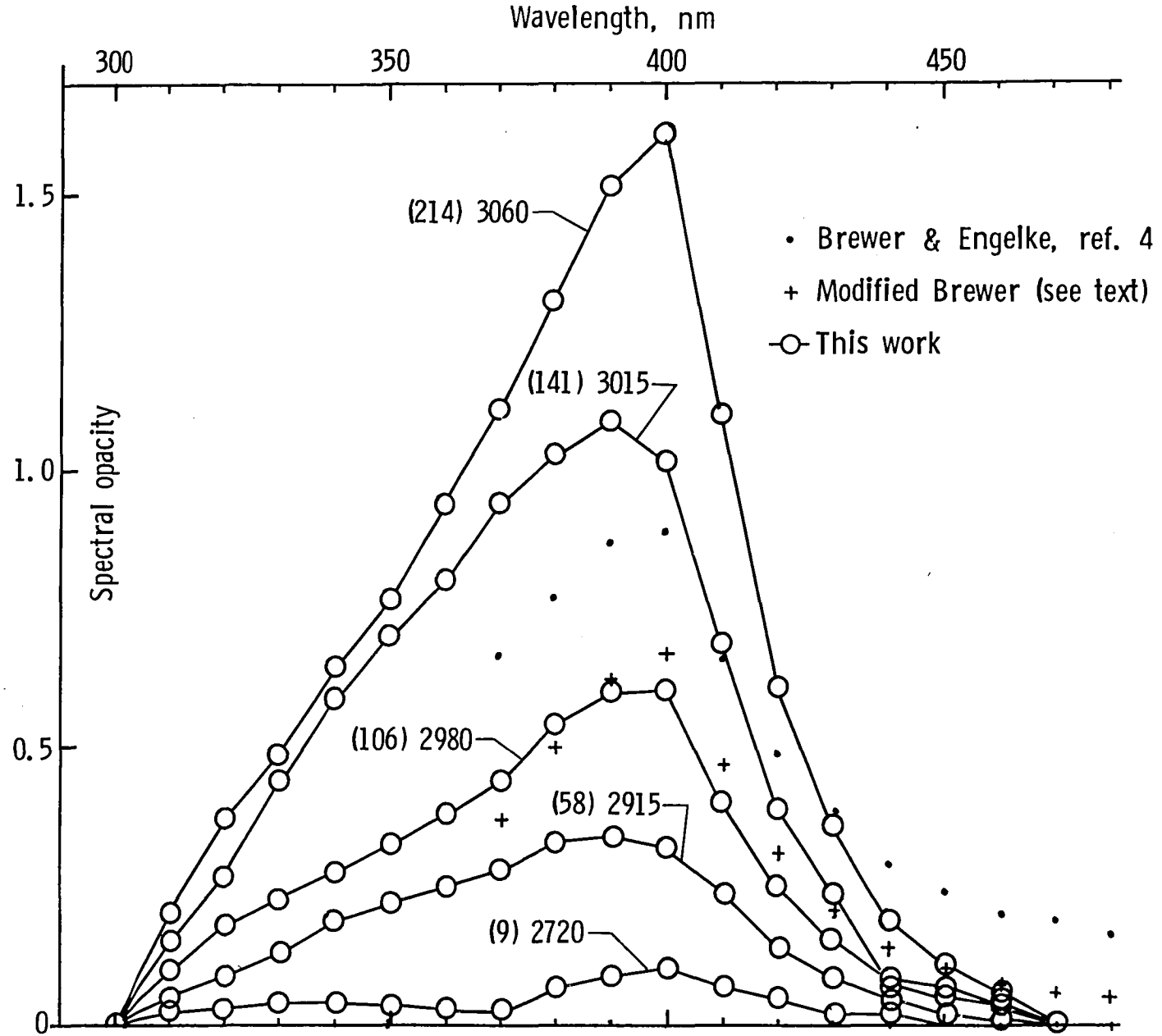

Figure 5.- C_3 spectrum at different opacity levels. Numbers in parentheses correspond to the measured integrated absorption cm^{-2} of the $\Delta v = 0$ C_2 Swan system associated with the data and the temperature represents t_c in centigrade.

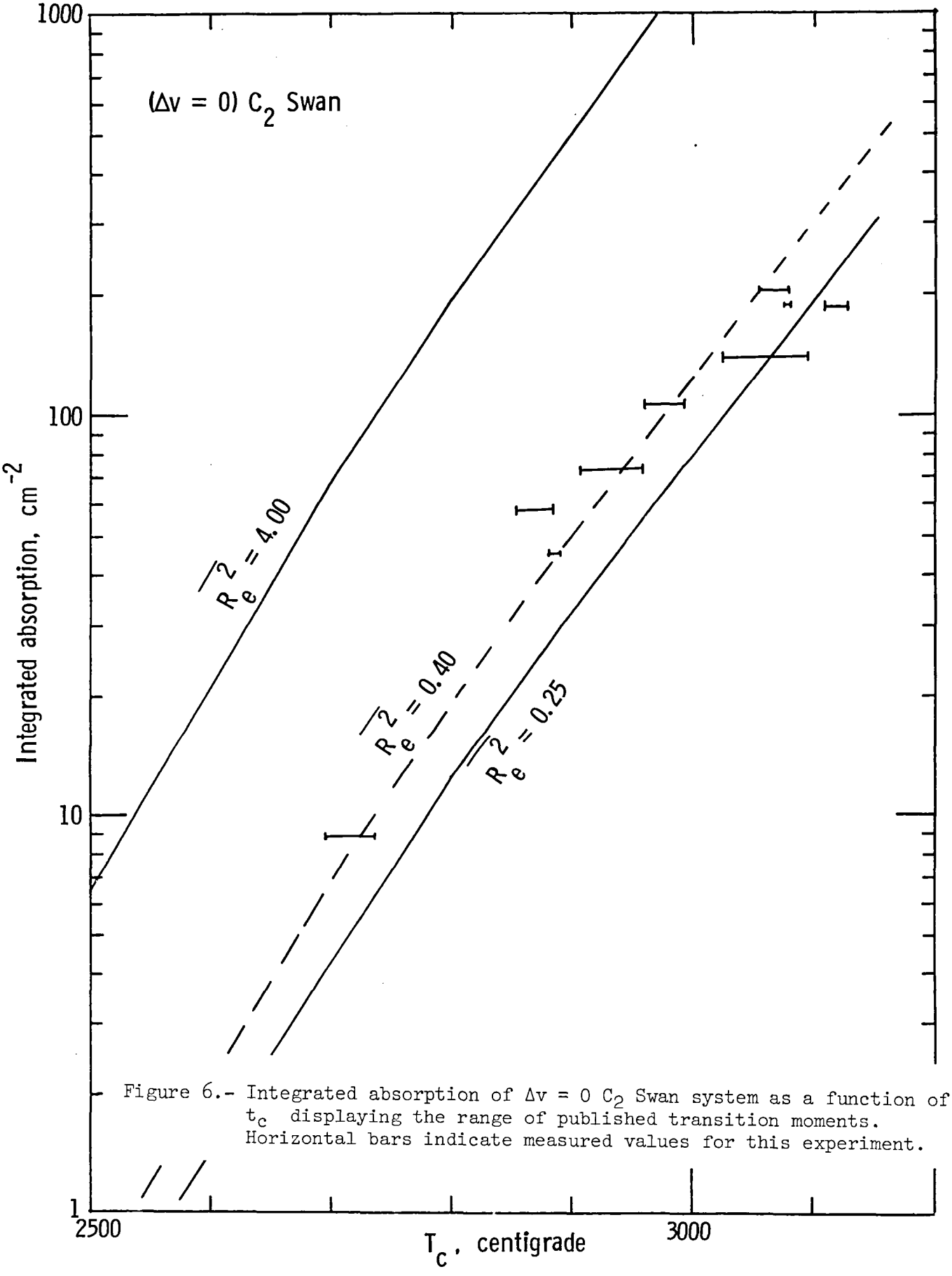

Figure 6.- Integrated absorption of $\Delta v = 0$ C_2 Swan system as a function of t_c displaying the range of published transition moments. Horizontal bars indicate measured values for this experiment.

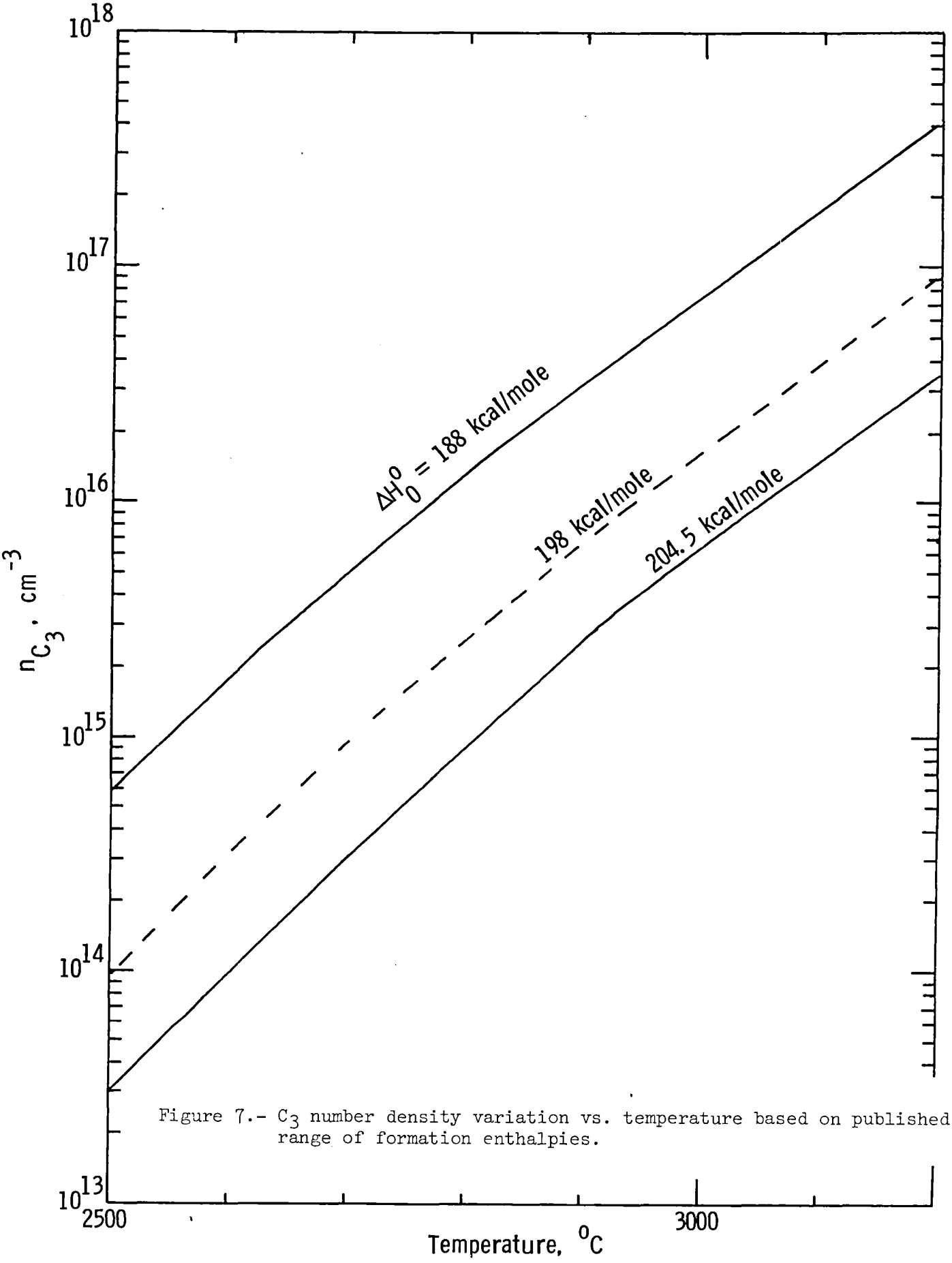

Figure 7.- C_3 number density variation vs. temperature based on published range of formation enthalpies.

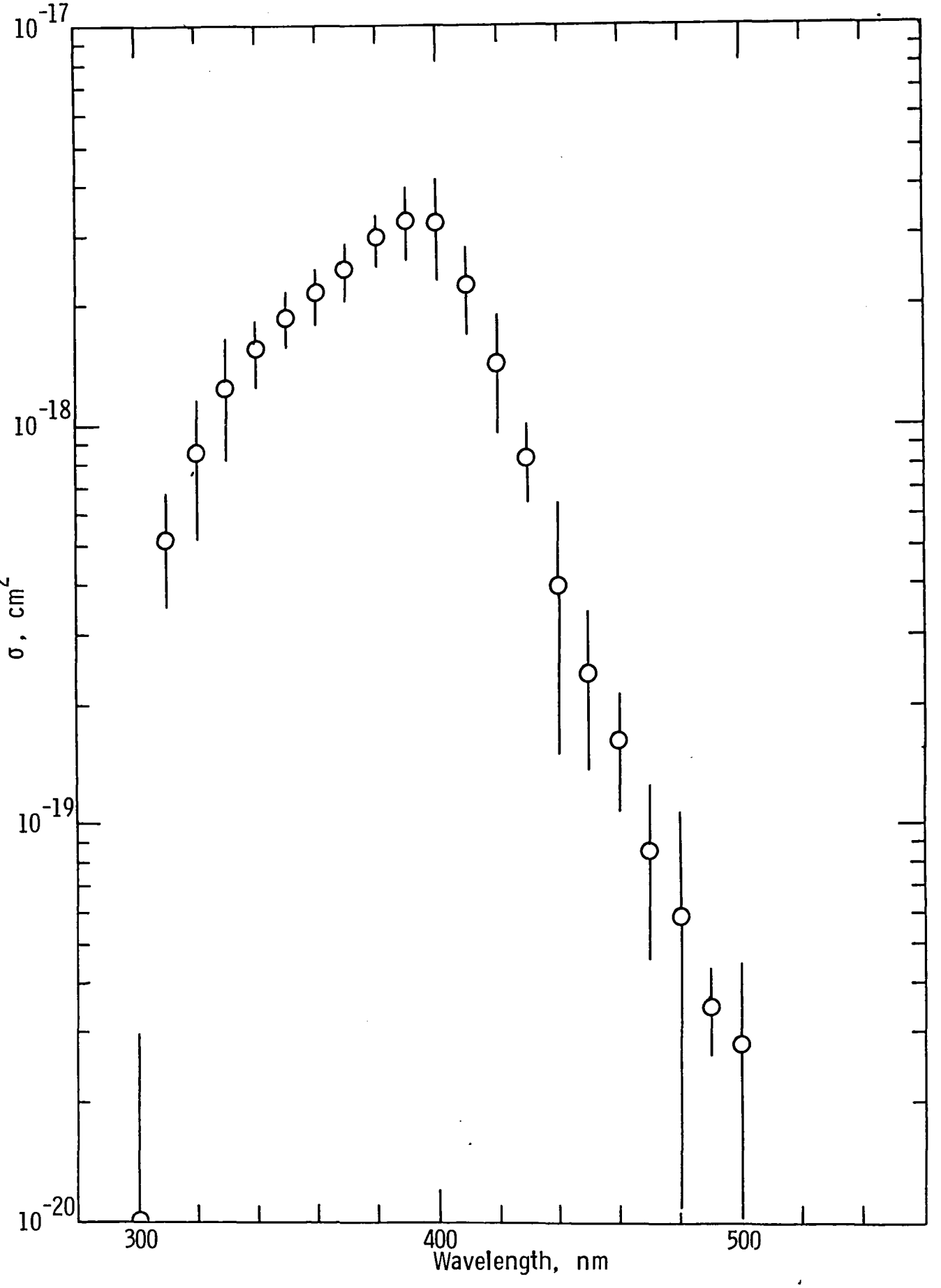

Figure 8.- Measured C_3 cross section. Bars indicate one standard deviation scatter.

1. Report No.	2. Government Accession No.	3. Recipient's Catalog No.
NASA TM-81837		

4. Title and Subtitle	5. Report Date
The Spectral Opacity of Triatomic Carbon Measured in a Graphite Tube Furnace Over the 280 to 600 nm Wavelength Range	July 1980
	6. Performing Organization Code
7. Author(s)	8. Performing Organization Report No.
Walter L. Snow and William L. Wells	
9. Performing Organization Name and Address	10. Work Unit No.
Langley Research Center Hampton, Virginia 23665	506-51-23-02
	11. Contract or Grant No.
	13. Type of Report and Period Covered
12. Sponsoring Agency Name and Address	Technical Memorandum
National Aeronautics and Space Administration Washington, DC 20546	14. Sponsoring Agency Code

15. Supplementary Notes

16. Abstract

The opacity of linear triatomic carbon (C_3) was measured in a graphite tube furnace from 280 to 600 nm to supplement the earlier measurements of Brewer and Engelke. The spectral cross section was estimated from the opacities using temperature profiles determined pyrometrically and a revised heat of formation (ΔH_0° = 198 kcal/mole). The cross section was found to be nonnegligible over the range 300-500 nm and the electronic oscillator strength based on the total cross section estimate was 0.02.

17. Key Words (Suggested by Author(s))	18. Distribution Statement
Triatomic Carbon Spectral Absorption Cross Section Radiative Heat Transfer Carbon Vapor	Unclassified - Unlimited Subject Category 25

19. Security Classif. (of this report)	20. Security Classif. (of this page)	21. No. of Pages	22. Price*
Unclassified	Unclassified	22	A02

* For sale by the National Technical Information Service, Springfield, Virginia 22161